Flow Turbulence Combust (2006) 77: 277–303
DOI 10.1007/s10494-006-9047-1

Transition Modelling for General Purpose CFD Codes

F. R. Menter · R. Langtry · S. Völker

Accepted: 21 March 2006 / Published online: 18 August 2006
© Springer Science + Business Media B.V. 2006

Abstract The paper addresses modelling concepts based on the RANS equations for laminar-turbulent transition prediction in general-purpose CFD codes. Available models are reviewed, with emphasis on their compatibility with modern CFD methods. Requirements for engineering transition models suitable for industrial CFD codes are specified. A new concept for transition modeling is introduced. It is based on the combination of experimental correlations with locally formulated transport equations. The concept is termed LCTM – Local Correlation-based Transition Model. An LCTM model, which satisfies most of the specified requirements is described, including results for a variety of different complex applications. An incremental approach was used to validate the model, first on 2D flat plates and airfoils and then on to progressively more complicated test cases such as a three-element flap, a 3D transonic wing and a full helicopter configuration. In all cases good agreement with the available experimental data was observed. The authors believe that the current formulation is a significant step forward in engineering transition modeling, as it allows the combination of transition correlations with general purpose CFD codes. There is a strong potential that the model will allow the 1st order effects of transition to be included in everyday industrial CFD simulations.

Key words laminar-turbulent transition · intermittency · local formulation · turbulence modelling · transport equation · SST model · LCTM

F. R. Menter (✉) · R. Langtry
Software Development Dept., ANSYS-CFX Germany, 83624 Otterfing, Germany
e-mail: florian.menter@ansys.com

S. Völker
GE Global Research, One Research Circle, Niskayuna, NY 12309, USA

1. Introduction

In the last decades, significant progress has been made in the development of reliable turbulence models, which allow the accurate simulation of a wide range of fully turbulent engineering flows. The efforts by different groups have resulted in a spectrum of models, which can be used for different applications, while balancing the accuracy requirements and the computational resources available to a CFD user. However, the important effect of laminar-turbulent transition is not included in the large majority of today's engineering CFD simulations. The reason is that transition modelling does not offer the same wide spectrum of CFD-compatible model formulations as available for turbulent flows, although a large body of publications is available on the subject. There are several reasons for this unsatisfactory situation.

The first is that transition occurs through different mechanisms in different applications. In aerodynamic flows, transition is typically a result of a flow instability (Tollmien–Schlichting waves or cross-flow instability), where the resulting exponential growth eventually results in a nonlinear breakdown to turbulence. In turbomachinery applications, the main transition mechanism is bypass transition [11, 18] imposed on the boundary layer by high levels of turbulence in the free stream, coming from the upstream blade rows. Another important transition mechanism is separation-induced transition [12], where a laminar boundary layer separates under the influence of a pressure gradient and transition develops within the separated shear layer (which may or may not reattach). Finally, an already turbulent boundary layer can relaminarise under a strong favourable pressure gradient [10]. While the importance of transition phenomena for aerodynamic and heat transfer simulations is widely accepted, it is difficult to include all of these effects in a single model.

The second complication arises from the fact that the conventional (RANS) averaging procedures do not lend themselves easily to the description of transitional flows, where both, linear and nonlinear effects are relevant. RANS averaging eliminates the effects of linear disturbance growth and is therefore difficult to apply to the transition process. While methods based on the stability equations, like the e^n method of Smith and Gamberoni [27] and van Ingen [36] avoid this limitation, they are not compatible with general-purpose CFD methods as typically applied in complex geometries. The reason is that these methods require a priori knowledge of the geometry and the grid topology. In addition, they involve numerous nonlocal operations, which are not easily implemented into today's CFD methods [31]. This is not to argue against these models, which are an essential part of the desired 'spectrum' of transition models required for the vastly different application areas and accuracy requirements. However, much like in turbulence modelling, it is important to develop engineering models, which can be applied in the day-to-day operation by design engineers on varying geometries.

Closer inspection shows that hardly any of the current transition models are CFD-compatible. Most formulations suffer from nonlocal operations, which cannot be carried out (with reasonable effort) in a general-purpose CFD code. It has to be understood that modern CFD codes do not provide the infrastructure of computing integral boundary layer parameters, or allow the integration of quantities along the direction of external streamlines. Even if structured boundary layer grids are used (typically hexahedra or prism layers), the codes are based on data structures for unstructured meshes. The information on a body-normal grid direction is therefore not easily available. In addition, industrial CFD simulations are carried out on

parallel computers using a domain decomposition methodology. This means in the most general case that boundary layers are typically split and computed on different processors, prohibiting any search or integration algorithms. Furthermore, for general purpose CFD applications, the grid topology relative to the surfaces is not known a priori, as the user has the freedom to freely choose both, geometry and grid topologies. The main requirements for a fully CFD-compatible transition model are therefore:

1. Allow the *calibrated* prediction of the onset and the length of transition.
2. Allow the inclusion of the different transition mechanisms.
3. Be formulated locally (no search or line-integration operations).
4. Avoid multiple solutions (same solution for initially laminar or turbulent boundary layer).
5. Do not affect the underlying turbulence model in fully turbulent regimes.
6. Allow a robust integration with similar convergence as underlying turbulence model.
7. Be formulated independent of the coordinate system.

Considering the main classes of engineering transition models (stability analysis, correlation based models, low-Re models) one finds that most of these methods lack one or the other of the above requirements.

The only formulations, which have historically been compatible with CFD methods, are low-Re models [3, 19]. However, they typically suffer from the close interaction of the transition capability and the viscous sublayer modelling, which prevents an independent calibration of both phenomena [22]. In addition, low-Re models can at best be expected to simulate bypass transition, which is dominated by diffusion effects. From a global perspective (without accounting for the differences between different models in the same group), standard low-Re models rely on the ability of the wall damping terms to also capture some of the effects of transition. Realistically, it would be surprising if models calibrated for viscous sublayer damping would faithfully reproduce the many effects of transitional flows. It is understandable that models using damping functions based on the turbulent Reynolds number have some transition characteristics. Nevertheless, the effect is best described as 'pseudo-transition,' as it was never actually built into the model. However, there are several models, where transition prediction was considered during model calibration [8, 37, 38]. It is interesting to note that several of these models use the strain-rate (or vorticity-rate) Reynolds number Re_V as an indicator for estimating the state of the laminar boundary layer. Nevertheless, these model formulations are based on a close connection of the sublayer and the transition calibration. Re-calibration of one model functionality also changes the performance of the other. It is therefore not possible to introduce additional experimental information, without a substantial re-formulation of the entire model. In most cases this operation can only be performed reliably by the model developer (or experts on model formulation). More complex models for transitional flows based on solving additional transport equations for either intermittency or pseudo laminar fluctuations have been developed by Steelant and Dick [29] and Lardeau et al. [9]. These models do however require a separate transition onset criteria, which is typically not formulated locally.

The engineering alternative to low-Re models are correlation-based formulations like those of Abu–Ghannam and Shaw [1], Mayle [10] and Suzen et al. [32]. They

typically correlate the transitional (momentum thickness) Reynolds number to local free-stream conditions, like turbulence intensity and pressure gradient. These models allow for an easy calibration and are often sufficiently accurate for capturing the major effects. In addition, correlations can be developed for the different transition mechanisms, ranging from bypass to natural transition to crossflow instability to separation induced transition. The main shortcoming of these models lies in their inherently nonlocal formulation. They typically require information on the integral thickness of the boundary layer and the state of the flow outside the boundary layer. While these models have been used successfully in special-purpose turbomachinery codes, the nonlocal operations have precluded their implementation into general-purpose CFD methods.

Transition simulations based on linear stability analysis, like the e^n method, are the lowest closure level, where the actual instability of the flow is simulated. However, even the e^n method is not free of empiricism, as the *n*-factor is not universal and depends on the wind tunnel or free-stream environment. The main obstacle to the use of the e^n model is however that the required infrastructure is typically very complex. The stability analysis is often based on velocity profiles obtained from highly resolved boundary layer codes, which are coupled to the pressure distribution of the RANS solver. The output of the boundary layer method is then transferred to a stability method, which then provides information back to the turbulence model in the RANS solver. The complexity of this set-up is mainly justified for special applications where the flow is designed to remain close to the stability limit for drag reduction, like laminar airplane wing design.

DNS and LES are suitable tools for transition prediction (e.g. [17, 39]), although even there, the proper specification of the external disturbance level and structure poses substantial challenges. These methods are far too costly for engineering applications, and are currently used mainly as research tools and substitutes for controlled experiments.

Despite its complexity, transition should not be viewed as outside the range of RANS methods. In many applications, transition is enforced within a narrow area of the flow by strong geometric disturbances, pressure gradients and/or flow separation. Even relatively simple models can capture these effects with sufficient engineering accuracy. The challenge to a proper engineering model is therefore mainly the formulation of models, which are suitable for implementation into a general RANS environment.

The present authors have recently developed a correlation-based transition model, built on transport equations, using only local variables. The concept is termed LCTM – Local Correlation-based Transition Model. The central idea behind this concept has been described in a model by Menter et al. [15]. The major numerical and modelling deficiencies associated with that prototype model have been eliminated by Menter et al. [16] and a wide range of turbomachinery-related flow problems has been computed by Langtry et al. [6]. The model has since been extended to aerodynamic flows [7] and is now run within the software package CFX-5, as well as the GE in-house code Tacoma on numerous industrial applications. The model satisfies all requirements given above, except for the last one – coordinate independence. This is a consequence of the fact that transition correlations are based on non-Galilean invariant parameters, like the turbulence intensity *Tu*. As boundary layer transition is always relative to walls, this is only an issue if multiple moving walls exist in a single computational domain. Efforts are underway for eliminating this restriction.

The model given in Menter et al. [16] and Langtry et al. [6] has been developed in a joint project between GE Global Research, ANSYS-CFX and the University of Kentucky. The model consists of two components. The first is the generic infrastructure provided by two transport equations, which link the CFD code to experimental correlations. The second component are the correlations themselves. The innovation lies in the generic infrastructure, which allows a direct coupling of general purpose CFD method with experimental transition data. The entire infrastructure of the formulation is given in Menter et al. [16] and will be repeated below. However, the model correlations were partly built on internal data and are not in the public domain. As the interfaces for the transitional correlations are clearly defined, other groups can use their own correlations as available for their application.

2. Strain-Rate Reynolds Number

Instead of using the momentum thickness Reynolds number to trigger the onset of transition, the current model is based on the strain-rate (or vorticity) Reynolds number, Re_v, [15, 35]:

$$\mathrm{Re}_v = \frac{\rho y^2}{\mu} S \tag{1}$$

where y is the distance from the nearest wall, ρ is the density, μ is the dynamic viscosity and S is the absolute value of the strain rate. Since the strain-rate Reynolds number depends only on density, viscosity, wall distance and the strain-rate (some formulations use the vorticity) it is a local property and can be easily computed at each grid point in an unstructured, parallel Navier–Stokes code.

A scaled profile of the strain-rate Reynolds number is shown in Figure 1 for a Blasius boundary layer. The scaling is chosen in order to have a maximum of one inside the boundary layer and is achieved by dividing the strain-rate Reynolds number profile from the Blasius solution by the corresponding momentum thickness Reynolds number and a constant of 2.193. In other words, the maximum of the profile

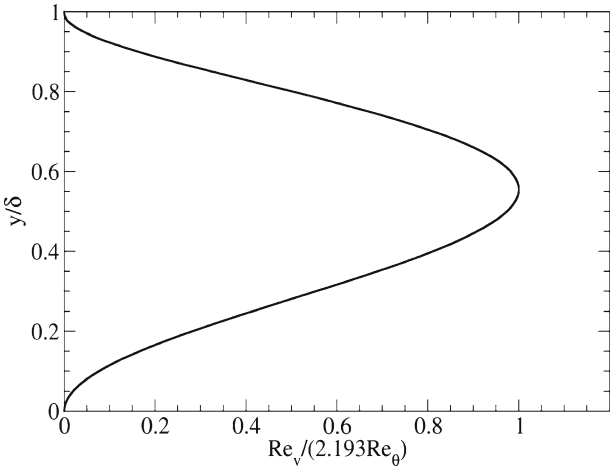

Figure 1 Scaled strain-rate Reynolds number (Re_v) profile in a Blasius boundary layer.

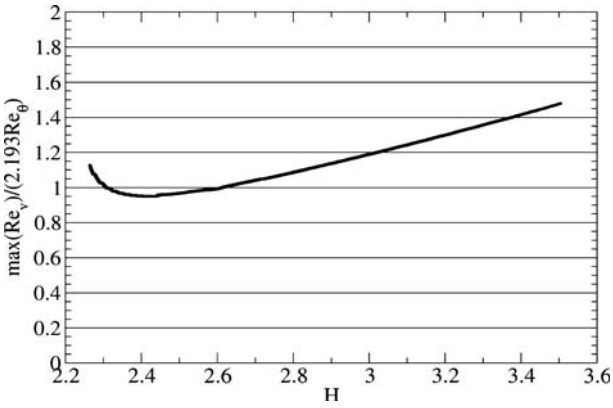

Figure 2 Relative error between the maximum value of strain-rate Reynolds number (Re_V) and the momentum thickness Reynolds number (Re_θ) as a function of boundary layer shape factor (H).

is proportional to the momentum thickness Reynolds number and can therefore be related to the transition correlations [15] as follows:

$$\mathrm{Re}_\theta = \frac{\max(\mathrm{Re}_v)}{2.193} \tag{2}$$

Based on this observation, a general framework can be built, which can serve as an environment for local correlation-based transition models (LCTM).

When the laminar boundary layer is subjected to strong pressure gradients, the relationship between momentum thickness and strain-rate Reynolds number described by Equation (2) changes due to the change in the shape of the profile. The relative difference between momentum thickness and strain-rate Reynolds number, as a function of shape factor (H), is shown in Figure 2. For moderate pressure gradients ($2.3 < H < 2.9$) the difference between the actual momentum thickness Reynolds number and the maximum of the strain-rate Reynolds number is less than 10%. Based on boundary layer analysis a shape factor of 2.3 corresponds to a pressure gradient parameter (λ_θ) of approximately 0.06. Since the majority of experimental data on transition in favourable pressure gradients falls within that range (see for example [1]) the relative error between momentum thickness and strain-rate Reynolds number is not of great concern under those conditions.

For strong adverse pressure gradients, the difference between the momentum thickness and strain-rate Reynolds number can become significant, particularly near separation ($H = 3.5$). This could either be accounted for by relating the proportionality factor to the local pressure gradient, or by including the effect directly into the correlations. The second approach is chosen in the current model.

3. The γ-Re_θ Transition Model

The main requirement for the transition model development was that only local variables and gradients, as well as the wall distance should be used in the equations. The wall distance can be computed from a Poisson equation and therefore does not break the paradigm of modern CFD methods. The present formulation avoids

another very severe shortcoming of the correlation-based models, namely their limitation to 2D flows. Already the definition of a momentum-thickness is strictly a 2D concept. It cannot be computed in general 3D flows such as a turbine blade with sidewall boundary layers. The current formulation avoids this shortcoming, and allows the simulation of 3D flows originating from different walls.

In the following section, a transport equation for the intermittency, γ, will be described in detail, which can be used to trigger transition locally. The intermittency function is coupled with the SST k-ω turbulence model [14]. It is used to turn on the production term of the turbulent kinetic energy downstream of the transition point in the boundary layer. This differs from the typical usage of intermittency (e.g. [34]) where the intermittency is often used to modify the eddy viscosity. However, from a modeling standpoint, the present approach has certain advantages (e.g. capturing the effect of large free-stream turbulence levels on laminar boundary layers and the related increase in the laminar skin friction and heat transfer). It should be noted that the transition model could in principle be used with a turbulence model other than SST (e.g. k-epsilon); however, this would most likely require a recalibration of some of the transition model constants. As well, one of the basic requirements of the underlying turbulence model is that it must produce full turbulent flow from the location where the model is first activated (i.e. Low-Reynolds number turbulence models which often predict some amount of laminar flow on their own could potentially affect the accuracy of the present transition model).

In addition to the transport equation for the intermittency, a second transport equation is solved in terms of the transition onset momentum-thickness Reynolds number ($\overline{\mathrm{Re}}_{\theta t}$). This is necessary in order to capture the nonlocal influence of the turbulence intensity, which changes due to the decay of the turbulent kinetic energy in the free-stream, as well as due to changes in the free-stream velocity outside the boundary layer. This additional transport equation is an essential part of the model as it ties the empirical correlation to the onset criteria in the intermittency equation and allows the model's use in general geometries and over multiple blades, without interaction from the user. As the transition model solves a transport equation for the intermittency, γ, and the transitional momentum thickness Reynolds number, Re_θ, the model was named the γ-Re_θ transition model. The γ-Re_θ model is one realization of an LCTM concept.

The formulation of the intermittency equation has been extended to account for the rapid onset of transition caused by separation of the laminar boundary layer. In addition, the model can be fully calibrated with in-house transition onset and transition length correlations. The correlations can also be extended to flows at low free-stream turbulence intensity or to flows with cross-flow instability. The model formulation therefore offers a flexible environment for engineering transition predictions that is fully compatible with the infrastructure of modern CFD methods.

The present transition model formulation is described in five sections. The first section details the formulation of the intermittency transport equation used to trigger the transition onset. The second section describes the new transport equation for the transition momentum thickness Reynolds number $\overline{\mathrm{Re}}_{\theta t}$, which is used to capture the nonlocal effect of free-stream turbulence intensity and pressure gradient at the boundary layer edge. The third section describes a modification that is used to improve the predictions for separated flow transition. The fourth section gives an overview of the correlations, which have to be supplied with the model. The fifth section describes the link between the transition model and the SST model.

3.1. Transport equation for intermittency

A new transport equation for the intermittency, γ, has been developed. The equation is built on the one given by Menter et al. [15] but corrects most of the deficiencies of that early formulation. A significant change to the formulation given by Menter et al. [15] is that the intermittency is now set to be equal to one in the free stream, instead of a small value as in the original model. This differs from the usual definition of intermittency where the free stream intermittency is usually zero and is only equal to one in turbulent boundary layers. However, the present approach has several advantages, especially in stagnation regions and near the boundary layer edge, where the original formulation did interfere with the turbulence model. The concept of a non-zero free stream intermittency has previously been employed by Steelant and Dick [30] in their intermittency transport equation. Although physical arguments can be made for this modification (at least for bypass transition, where the turbulence is diffused into the boundary layer from high free stream levels) it is mainly used here to extend the applicability and robustness of the current method. In addition, the empirical correlations for transition onset are applicable only for predicting boundary layer transition, not free shear transition (i.e. a laminar jet transitioning to a turbulent jet). As a result, away from walls, the transition model should enforce the fully turbulent behaviour of the turbulence model.

The intermittency equation is formulated as follows:

$$\frac{\partial(\rho\gamma)}{\partial t} + \frac{\partial\left(\rho U_j \gamma\right)}{\partial x_j} = P_\gamma - E_\gamma + \frac{\partial}{\partial x_j}\left[\left(\mu + \frac{\mu_t}{\sigma_f}\right)\frac{\partial\gamma}{\partial x_j}\right] \tag{3}$$

The transition source term is defined as:

$$P_{\gamma 1} = F_{length} c_{a1} \rho S\left[\gamma F_{onset}\right]^{0.5}(1-\gamma) \tag{4}$$

where S is the strain rate magnitude. This term is designed to be equal to zero (due to the F_{onset} function) in the laminar boundary layer upstream of transition and active wherever the local strain-rate Reynolds number exceeds the local transition onset criteria. The magnitude of this source term is controlled by the transition length function (F_{length}). The last term in Equation (4) is used to limit the maximum value of the intermittency so that it cannot exceed a value of one.

One of the main differences to other intermittency models lies in the formulation of the function F_{onset}, which is used to trigger the intermittency production (i.e. activate Equation 4). It is designed to switch rapidly from a value of zero in a laminar boundary layer to a value of one downstream of transition onset. It is formulated as a function of the local strain-rate Reynolds number Re_{v} and the turbulent Reynolds number Re_{T}:

$$\mathrm{Re}_V = \frac{\rho y^2 S}{\mu}; \quad R_T = \frac{\rho k}{\mu\omega} \tag{5}$$

$$F_{onset1} = \frac{\mathrm{Re}_v}{2.193 \cdot \mathrm{Re}_{\theta c}} \tag{6}$$

$$F_{onset2} = \min\left(\max\left(F_{onset1}, F_{onset1}^4\right), 2.0\right) \tag{7}$$

$$F_{onset3} = \max\left(1 - \left(\frac{R_T}{2.5}\right)^3, 0\right) \tag{8}$$

$$F_{onset} = \max\left(F_{onset2} - F_{onset3}, 0\right) \tag{9}$$

One of the problems observed with the F_{onset2} function was that during the transition process the strain-rate Reynolds number would actually decrease due to the change in the velocity profile. This could cause the transition process to stall. As a result, the viscosity ratio was introduced in Equation (8) in order to help ensure that the F_{onset} function was active throughout the transitional region. The rational behind this equation is given in more detail in Menter et al. [15]. $Re_{\theta c}$ in Equation (6) is the critical Reynolds number where the intermittency first starts to increase in the boundary layer. This occurs upstream of the transition Reynolds number, $Re_{\theta t}$ because there is a delay due to the fact that the turbulence must first build up to appreciable levels in the boundary layer before any change in the laminar profile can occur. As a result, $Re_{\theta c}$ can be thought of as the location where turbulence starts to grow while $Re_{\theta t}$ is the location where the velocity profile first starts to deviate from the purely laminar profile. The connection between the two must be obtained from an empirical correlation where:

$$\text{Re}_{\theta c} = f\left(\overline{\text{Re}}_{\theta t}\right) \tag{10}$$

and $\overline{\text{Re}}_{\theta t}$ comes from the transport equation given by Equation (16). This correlation is determined based on a series of numerical experiments on a flat plate where the critical Reynolds number was varied along with the free stream turbulence intensity and the subsequent transition Reynolds number was measured based on the most upstream location where the skin friction started to increase.

F_{length} in Equation (4) is an empirical correlation that controls the length of the transition region. It is based on a significant amount of numerical experimentation whereby a series of flat plate experiments where reproduced and a curve fitting program was used to develop a correlation that resulted in the correct prediction of the transition length as compared to experimental data. Once the correct values for F_{length} where determined (as a function of transition Reynolds number) these values where used to develop a correlation so that the transition length could be correctly reproduced over the whole range of Reynolds numbers. It should be noted that the $Re_{\theta c}$ and F_{length} correlations are strong functions of each other and there was a significant amount of iteration required in order to obtain good agreement between both correlations. The F_{length} correlation is also defined as a function of $\overline{\text{Re}}_{\theta t}$:

$$F_{length} = f\left(\overline{\text{Re}}_{\theta t}\right) \tag{11}$$

The destruction/relaminarization source is defined as follows:

$$E_\gamma = c_{a2}\rho\Omega\gamma F_{turb}\left(c_{e2}\gamma - 1\right) \tag{12}$$

where Ω is the vorticity magnitude. This term acts like a sink term and ensures that the intermittency remains close to zero ($1/c_{e2}$) in the laminar boundary layer [it is one in the free stream due to the inlet boundary condition and also due the presence of wall distance in Equation (6)]. It also enables the model to predict relaminarisation because it provides a means for the intermittency to return to zero, once the transition criteria in the F_{onset} function is no longer satisfied (e.g. an accelerated boundary layer

that becomes thin enough to relaminarise). The constant c_{a2} controls the strength of the destruction term and ensures that the entire term is smaller then the transition source term $P\gamma$. This allows the transition source term to overwhelm the destruction term once the onset criteria is satisfied. The constant c_{e2} controls the lower limit of intermittency, where the term changes sign. The value of 50 results in a lower limit of 0.02, which is small enough to keep the boundary layer laminar. The vorticity was used in the destruction term in order of avoiding the destruction of intermittency in the free stream due to free-stream strain rates.

F_{turb} is used to disable the destruction/relaminarization source in the fully turbulent regime:

$$F_{turb} = e^{-\left(\frac{R_T}{4}\right)^4} \tag{13}$$

The constants for the intermittency equation are:

$$c_{a1} = 2.0; \quad c_{e2} = 50; \quad c_{a2} = 0.06; \quad \sigma_f = 1.0; \tag{14}$$

The boundary condition for γ at a wall is zero normal flux. At an inlet, the value of γ is equal to 1. In order to capture the laminar and transitional boundary layers correctly, the grid must have a y^+ of approximately 1. If the y^+ is too large (i.e. > 5) than the transition onset location moves upstream with increasing y^+. It has also been determined that the transition onset location is sensitive to the advection scheme used for the turbulence and transition model equations. For this reason all equations were solved with a bounded high resolution (i.e. a limited second order) upwind scheme. This resulted in grid independent solutions on reasonable sized grids (e.g. for a turbine blade, 200 nodes around the blade, y^+ of 1 with a wall normal grid expansion ratio of 1.1–1.15).

3.2. Transport equation for transition momentum thickness Reynolds number

The experimental transition correlations relate the Reynolds number of transition onset, $Re_{\theta t}$, to the turbulence intensity, Tu, and other quantities in the free stream where:

$$\text{Re}_{\theta t} = f(Tu, ...)_{freestream} \tag{15}$$

This is a nonlocal operation, as the value of $Re_{\theta t}$ is required by the intermittency equation inside the boundary layer, and not only in the free stream. It should also be noted that the turbulence intensity can change strongly in a domain and that one global value over the entire flowfield is therefore not acceptable. Examples of such flows are highly loaded transonic turbomachinery or unsteady-state rotor-stator interactions. Since the main requirement for the current transition model is that only local quantities can be used, there must be a means of passing the information about the free-stream conditions into the boundary layer.

The following transport equation can be used to resolve this issue using a local formulation. The basic concept is to treat the transition momentum thickness Reynolds number, $Re_{\theta t}$, as a transported scalar quantity. The idea is then to use an empirical correlation to calculate $Re_{\theta t}$ in the free stream and to allow the free stream value to diffuse into the boundary layer. This is possible because the empirical correlations are defined as $Re_{\theta t} = f(Tu, dp/ds)$, and since Tu and dp/ds (streamwise pressure gradient) are defined in the free stream, $Re_{\theta t}$ is the only unknown quantity in the equation. This

transport equation essentially takes a nonlocal empirical correlation and transforms it into a local quantity, which can then be used to compute the transition length [F_{length}, Equation (11)] and critical Reynolds number [$Re_{\theta c}$, Equation (10)] at every location in the flow field. The intermittency equation [Equation (3)] can then be solved like a regular transport equation because the source terms are now local.

The transport equation for the transition momentum thickness Reynolds number ($\overline{\text{Re}}_{\theta t}$) is defined as follows:

$$\frac{\partial\left(\rho\overline{\text{Re}}_{\theta t}\right)}{\partial t}+\frac{\partial\left(\rho U_j\overline{\text{Re}}_{\theta t}\right)}{\partial x_j}=P_{\theta t}+\frac{\partial}{\partial x_j}\left[\sigma_{\theta t}(\mu+\mu_t)\frac{\partial\overline{\text{Re}}_{\theta t}}{\partial x_j}\right] \tag{16}$$

Outside the boundary layer, the source term $P_{\theta t}$ is designed to force the transported scalar $\overline{\text{Re}}_{\theta t}$ to match the local value of $Re_{\theta t}$ calculated from an empirical correlation. The source term is defined as follows:

$$P_{\theta t}=c_{\theta t}\frac{\rho}{t}\left(\text{Re}_{\theta t}-\overline{\text{Re}}_{\theta t}\right)(1.0-F_{\theta t}) \tag{17}$$

$$t=\frac{500\mu}{\rho U^2} \tag{18}$$

where t is a time scale, which is present for dimensional reasons. The time scale was determined based on dimensional analysis with the main criteria being that it had to scale with the convective and diffusive terms in the transport equation. The blending function $F_{\theta t}$ is used to turn off the source term in the boundary layer and allows the transported scalar $\overline{\text{Re}}_{\theta t}$ to diffuse in from the free stream. $F_{\theta t}$ is equal to zero in the free stream and one in the boundary layer. The $F_{\theta t}$ blending function is defined as follows:

$$F_{\theta t}=\min\left(\max\left(F_{wake}\cdot e^{-\left(\frac{y}{\delta}\right)^4},1.0-\left(\frac{\gamma-1/c_{e2}}{1.0-1/c_{e2}}\right)^2\right),1.0\right) \tag{19}$$

$$\theta_{BL}=\frac{\overline{\text{Re}}_{\theta t}\mu}{\rho U}\qquad \delta_{BL}=\frac{15}{2}\theta_{BL}\qquad \delta=\frac{50\Omega y}{U}\cdot\delta_{BL} \tag{20}$$

$$\text{Re}_{\omega}=\frac{\rho\omega y^2}{\mu} \tag{21}$$

$$F_{wake}=e^{-\left(\frac{\text{Re}_{\omega}}{1\times10^5}\right)^2} \tag{22}$$

The F_{wake} function ensures that the blending function is not active in the wake regions downstream of an airfoil/blade. The boundary condition for $\overline{\text{Re}}_{\theta t}$ at a wall is zero flux. The boundary condition for $\overline{\text{Re}}_{\theta t}$ at an inlet is calculated from the empirical correlation based on the inlet turbulence intensity.

The model constants for the transport equation are as follows, where $c_{\theta t}$ controls the magnitude of the source term and $\sigma_{\theta t}$ controls the diffusion coefficient:

$$c_{\theta t}=0.03;\quad \sigma_{\theta t}=2.0 \tag{23}$$

There is some lag between changes in the free-stream value of $\overline{\text{Re}}_{\theta t}$ and that inside the boundary layer. The lag is desirable, as according to Abu–Ghannam and Shaw [1] the onset of transition is primarily affected by the past history of pressure gradient and

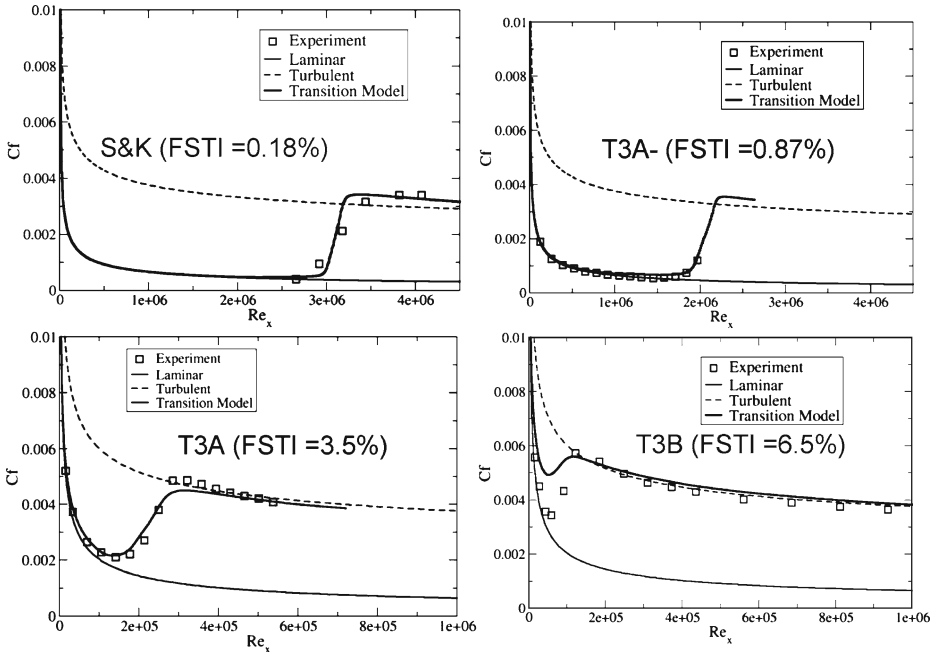

Figure 3 Results for flat plate test cases with different freestream turbulence levels (FSTI – Freestream Turbulence Intensity).

turbulence intensity and not the local value at transition. The lag between the local value of $\overline{\mathrm{Re}}_{\theta t}$ in the boundary layer and that in the free stream can be controlled by the diffusion coefficient $\sigma_{\theta \mathrm{t}}$. The larger the value of $\sigma_{\theta \mathrm{t}}$ the less sensitive the transition model is to history effects. The present value of $\sigma_{\theta \mathrm{t}} = 2$ was obtained based on the T3 series of flat plate transition experiments (Figures 3 and 4) were the free stream turbulence intensity and pressure gradient were rapidly changing and flow history effects are believed to be significant.

3.3. Separation induced transition

It became apparent during the development of the present transition model that whenever a laminar boundary layer separation occurred, the model consistently predicted the turbulent reattachment location too far downstream. Based on experimental results for a low-pressure turbine blade the agreement with experimental data tended to decrease as the free stream turbulence intensity was lowered. Presumably this is because the turbulent kinetic energy, k, in the separating shear layer is smaller at lower free stream turbulence intensities. As a result, it takes longer for k to grow to large enough values that would cause the boundary layer to reattach. This is the case even if the onset of transition is predicted at or near the separation point.

To correct this deficiency, a modification to the transition model was introduced that allows k to grow rapidly once the laminar boundary layer separates. The modification has been formulated so that it has a negligible effect on the predictions for attached transition or fully turbulent flow. The main idea behind the separation-

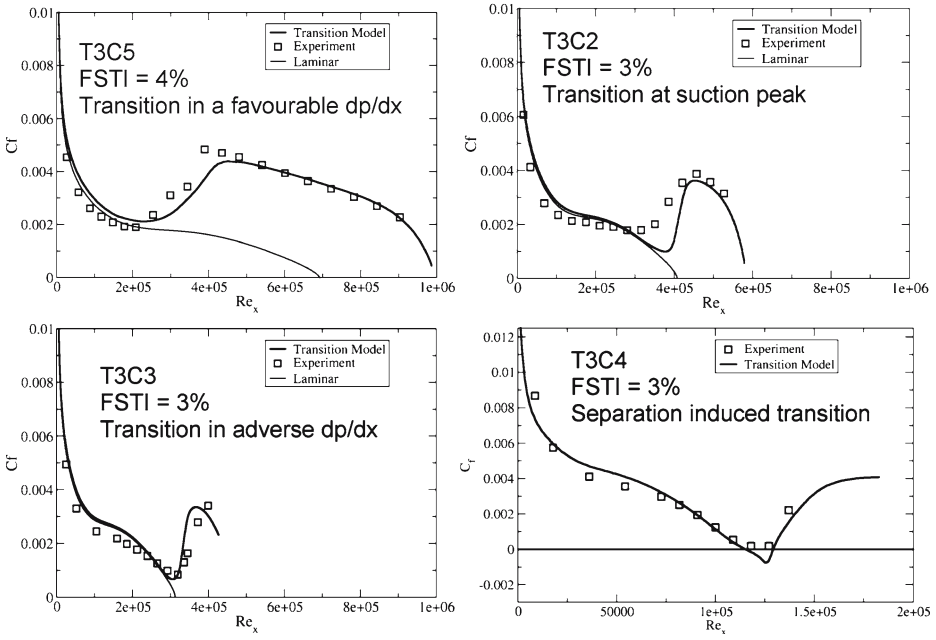

Figure 4 Results for flat plate test cases where variation of the tunnel Reynolds number causes transition to occur in different pressure gradients (dp/dx).

induced transition correction is to allow the local intermittency to exceed 1 whenever the laminar boundary layer separates. This will result in a large production of k, which in turn will cause earlier reattachment. The means for accomplishing this is based on the fact that for a laminar separation the strain-rate Reynolds number Re_{v} significantly exceeds the critical momentum thickness Reynolds number $Re_{\theta \mathrm{c}}$. As a result, the ratio between the two (when $Re_{\mathrm{v}} > Re_{\theta \mathrm{c}}$) can be thought of as a measure of the size of the laminar separation and can therefore be used to increase the production of turbulent kinetic energy. The modification for separation-induced transition is given by:

$$\gamma_{sep} = \min\left(s_1 \max\left[0, \left(\frac{\mathrm{Re}_v}{3.235\,\mathrm{Re}_{\theta c}}\right) - 1\right] F_{reattach}, 2\right) F_{\theta t} \quad (24)$$

$$F_{reattach} = e^{-\left(\frac{R_T}{20}\right)^4} \quad (25)$$

$$\gamma_{eff} = \max\left(\gamma, \gamma_{sep}\right) \quad (26)$$

$$s_1 = 2$$

The size of the separation bubble can be controlled with the constant s_1. F_{reattach} disables the modification once the viscosity ratio is large enough to cause reattachment. $F_{\theta \mathrm{t}}$ is the blending function from the $\overline{\mathrm{Re}}_{\theta t}$ equation [Equation (16)] and confines the modification to boundary layer flows. The constant 3.235 is the relation between Re_{v} and Re_{θ} for a shape factor (H) equal to 3.5 (i.e. at the separation point, see Figure 2).

The ability to include such a complex effect as separation-induced transition in such a simple way into the model shows the flexibility of the current approach.

3.4. Empirical correlations

The model contains three empirical correlations. $Re_{\theta t}$ is the transition onset as observed in experiments and it is used in Equation (17). F_{length} is the length of the transition zone and goes into Equation (4). $Re_{\theta c}$ is the point where the model is activated in order to match both, $Re_{\theta t}$ and F_{length}, and it goes into Equation (6).

$$\mathrm{Re}_{\theta t} = f(Tu, \lambda_\theta); \quad F_{length} = f\left(\overline{\mathrm{Re}}_{\theta t}\right); \quad \mathrm{Re}_{\theta c} = f\left(\overline{\mathrm{Re}}_{\theta t}\right) \tag{27}$$

The turbulence intensity, Tu, and Thwaites' pressure gradient coefficient, λ_θ, are defined as:

$$Tu = 100\frac{\sqrt{2k/3}}{U}; \quad \lambda_\theta = \frac{\rho\theta^2}{\mu}\frac{dU}{ds} \tag{28}$$

At present these empirical correlations are proprietary and cannot be given in the paper.

3.5. Coupling the transition model with the turbulence model

The Reynolds stresses and turbulent heat fluxes in the Navier–Stokes and energy equations are modeled using the eddy-viscosity/diffusivity approach. The eddy diffusivity in the energy equation is related to the eddy viscosity via the turbulent Prandtl number ($Pr_{\text{t}} = 0.9$). The eddy viscosity (μ_{t}) is calculated from the following modified version of the SST turbulence model [14] as follows:

$$\mu_t = \min\left[\frac{\rho k}{\omega}; \frac{a_1 \rho k}{SF_2}\right] \tag{29}$$

$$\frac{\partial}{\partial t}(\rho k) + \frac{\partial}{\partial x_j}(\rho u_j k) = \tilde{P}_k - \tilde{D}_k + \frac{\partial}{\partial x_j}\left((\mu + \sigma_k \mu_t)\frac{\partial k}{\partial x_j}\right) \tag{30}$$

$$\frac{\partial}{\partial t}(\rho \omega) + \frac{\partial}{\partial x_j}(\rho u_j \omega) = \alpha\frac{P_k}{\nu_t} - D_\omega + Cd_\omega + \frac{\partial}{\partial x_j}\left((\mu + \sigma_k \mu_t)\frac{\partial \omega}{\partial x_j}\right) \tag{31}$$

$$\tilde{P}_k = \gamma_{eff} P_k; \qquad \tilde{D}_k = \min\left(\max(\gamma_{eff}, 0.1), 1.0\right) D_k \tag{32}$$

where P_{k} and D_{k} are the production and destruction terms from the turbulent kinetic energy equation. The only difference between these equations and the original SST model is the appearance of the effective intermittency [γ_{eff}, see Equation (26)] in Equation (32). It should be stressed that the intermittency is used only to control the source terms in the k-equation, it is not used to multiply the eddy viscosity [Equation (29)]. In this way the present concept of intermittency is somewhat different than the standard definition used by Steelant and Dick [30] or Suzen et al. [32]. However, the present approach has two main advantages. The first is that it improves the robustness of the model because the intermittency does not enter directly into the momentum equations. The second advantage is that it allows the model to predict the effects of high free stream turbulence levels on buffeted laminar

boundary layers. The reason is that for large free stream eddy viscosities, the small values of intermittency in the boundary layer do not cancel out the local eddy viscosity. Consequently, the increase in the laminar shear stress and heat transfer that has been observed experimentally in buffeted laminar boundary layers can in principle, be captured by the present model.

One further modification to the SST turbulence model is a change in the blending function F_1 responsible for switching between the k-ω and k-ε models. It was found that in the center of the laminar boundary layer F_1 could potentially switch from 1.0 to 0.0. This is not desirable, as the k-ω model must be active in the laminar and transitional boundary layers. The deficiency in the blending function is not surprising as the equations used to define F_1 were intended solely for use in turbulent boundary layers. The solution is to redefine F_1 in terms of a blending function that will always be equal to 1.0 in a laminar boundary layer. The modified blending function is defined as follows:

$$R_y = \frac{\rho y \sqrt{k}}{\mu} \tag{33}$$

$$F_3 = e^{-\left(\frac{R_y}{120}\right)^8} \tag{34}$$

$$F_1 = \max\left(F_{1orig}, F_3\right) \tag{35}$$

where $F_{1\text{orig}}$ is the original blending function from the SST turbulence model.

4. Test Cases

The remaining part of the paper will give an overview of some of the public-domain test cases which have been computed with the model described above. This naturally requires a compact representation of the simulations. The cases are described in more detail in Menter et al. [16], Langtry et al. [6] and Langtry and Menter [7], including grid refinement and sensitivity studies.

4.1. Flat plate test cases

Test cases presented are the ERCOFTAC T3 series of flat plate experiments [20, 21, 22] and the Schubauer and Klebanof [24] flat plate experiment, all of which are commonly used as benchmarks for transition models. Also included is a test case where the boundary layer experiences a strong favourable pressure gradient that causes it to relaminarise [13].

The three cases (T3A, T3A and T3B) have zero pressure gradients with different free-stream turbulence intensity (FSTI) levels corresponding to transition in the bypass regime. The Schubauer and Klebanof (S&K) test case has a low free-stream turbulence intensity and corresponds to natural transition. Figure 3 shows the comparison of the model prediction with experimental data for theses cases. It also gives the corresponding FSTI values. In all simulations, the inlet turbulence levels were specified to match the experimental turbulence intensity and its decay rate. As the free-stream turbulence increases, the transition location moves to lower Reynolds numbers.

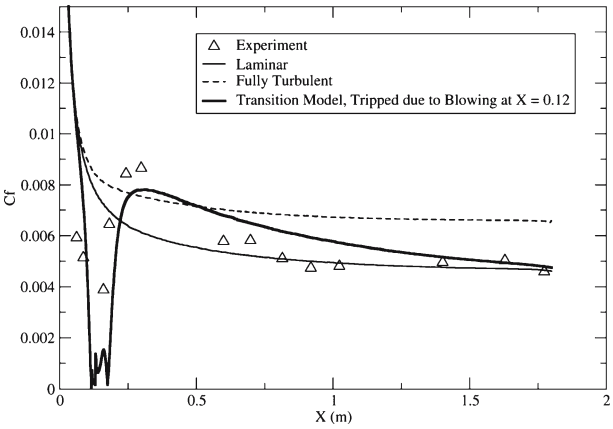

Figure 5 Predicted skin friction (Cf) for a flat plate with a strong acceleration that causes the boundary layer to relaminarize.

The T3C test cases consist of a flat plate with a favourable and adverse pressure gradient imposed by the opposite converging/diverging wall. The wind tunnel Reynolds number was varied for the four cases (T3C5, T3C3, T3C2, T3C4) thus moving the transition location from the favourable pressure at the beginning of the plate to the adverse pressure gradient at the end. The cases are used to demonstrate the transition models ability to predict transition under the influence of various pressure gradients. Figure 4 details the results for the pressure gradient cases. The effect of the pressure gradient on the transition length is clearly visible with favourable pressure gradients increasing the transition length and adverse pressure gradients reducing it. For the T3C4 case the laminar boundary layer actually separates and undergoes separation induced transition.

The relaminarisation test case is shown in Figure 5. For this case the opposite converging wall imposes a strong favourable pressure gradient that can relaminarise a turbulent boundary layer. In both the experiment and in the CFD prediction the boundary layer was tripped near the plate leading edge. In the CFD computation this was accomplished by injecting a small amount of turbulent air into the boundary layer. Downstream of the trip the boundary layer slowly relaminarises due to the strong favourable pressure gradient.

For all of the flat plate test cases the agreement with the data is generally good, considering the diverse nature of the physical phenomena computed, ranging from bypass transition to natural transition, separation-induced transition and even relaminarisation. Note that such a wide range of transition mechanisms is outside the scope of any other available transition model.

4.2. Turbomachinery test cases

4.2.1. *Zierke & Deutsch compressor cascade*

For the present test case [40], transition on the suction side occurs at the leading edge due to a small leading edge separation bubble on the suction side. On the pressure side, transition occurs at about mid-chord. The turbulence contours and the skin friction distribution are shown in Figure 6. There appears to be a significant amount of scatter in the experimental data, however, overall the transition model is predicting

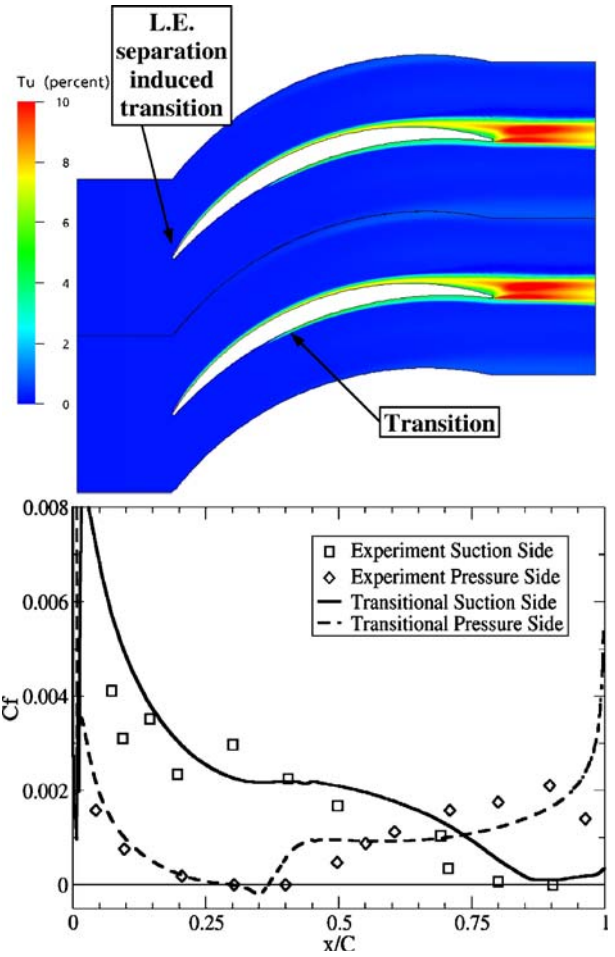

Figure 6 Turbulence intensity contours (*top*) and cf-distribution against experimental data (*right*) for the Zierke & Deutsch compressor.

the major flow features correctly (i.e. fully turbulent suction side, transition at mid-chord on the pressure side). One important issue to note is the effect of stream-wise grid resolution on resolving the leading edge laminar separation and subsequent transition on the suction side. If the number of stream-wise nodes clustered around the leading edge is too low, the model cannot resolve the rapid transition and a laminar boundary layer on the suction side is the result. For the present study, 60 streamwise nodes were used between the leading edge and the x/C equal to 0.1 location.

4.2.2. *Von-Karman institute turbine cascade*

The surface heat transfer for the transonic VKI MUR 241 (FSTI = 6.0%) and MUR 116 (FSTI = 1.0%) test cases [2] is shown in Figure 7. The strong acceleration on the suction side for the MUR 241 case keeps the flow laminar until a weak shock at mid chord, whereas for the MUR 116 case the flow is laminar until right before the trailing edge. Downstream of transition there appears to be a significant amount

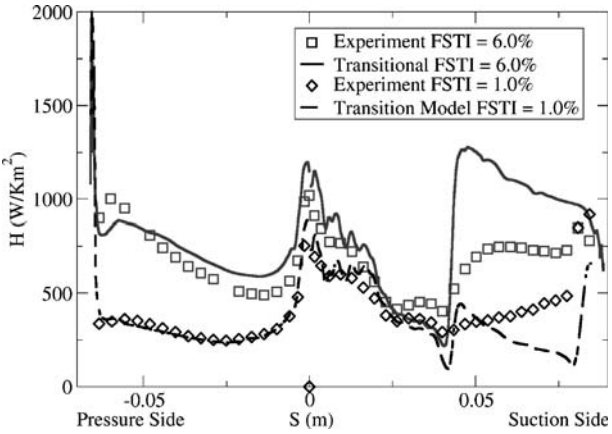

Figure 7 Heat transfer for the VKI MUR241 (FSTI = 6.0%) and MUR116 (FSTI = 1.0%) test cases.

of error between the predicted turbulent heat transfer and the measured value. It is possible that this is the result of a Mach number (inlet Mach number $Ma_{\text{inlet}} = 0.15$, $Ma_{\text{outlet}} = 1.089$) effect on the transition length [30, 31]. At present, no attempt has been made to account for this effect in the model. It can be incorporated in future correlations, if found consistently important.

The pressure side heat transfer is of particular interest for this case. For both cases, transition did not occur on the pressure side, however, the heat transfer was significantly increased for the high turbulence intensity case. This is a result of the large free-stream levels of turbulence which diffuse into the laminar boundary layer and increase the heat transfer and skin friction. From a modeling standpoint, the effect was caused by the large free-stream viscosity ratio necessary for MUR 241 to keep the turbulence intensity from decaying below 6%, which is the free-stream value quoted in the experiment. The enhanced heat transfer on the pressure side was also present in the experiment and the effect appears to be physical. The model can predict this effect, as the intermittency does not multiply the eddy-viscosity but only the production term of the k-equation. The diffusive terms are therefore active in the laminar region.

4.2.3. *RGW compressor cascade*

The RGW annular compressor [25] features a fully three-dimensional flow, including sidewall boundary layers originating upstream of the blade. This flow topology poses a major challenge to standard correlation-based transition models, as complex logic would be required to distinguish between the different boundary layers.

Figure 8 shows a comparison of the simulations on the suction side of the blade with an experimental oil-flow picture. For comparison, a fully turbulent flow simulation is also included. It can be seen that the transition model captures the complex flow topology of the experiments in good agreement with the data. A comparison between the transition model and the fully turbulent simulation shows the strong influence of the laminar flow separation on the sidewall boundary layer separation. The flow separation on the shroud is significantly reduced by the displacement effect of the separation bubble in the transitional simulation. As a result, the loss coefficient, $Yp = 0.19$, in the fully turbulent simulation is much higher than the experimental

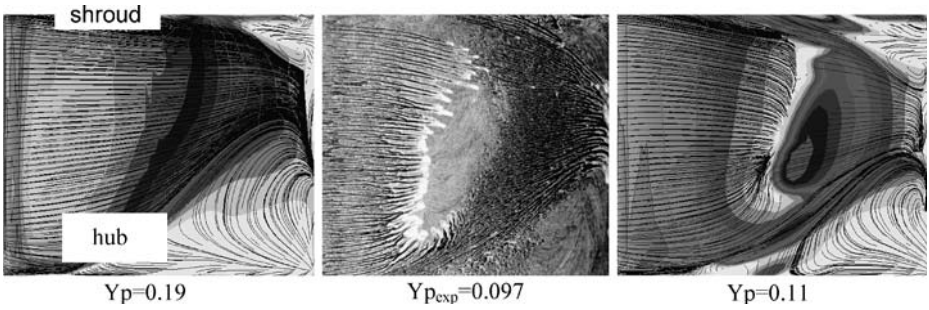

Figure 8 Fully turbulent (*left*) and transitional (*right*) skin friction on the suction side of the 3D RGW compressor cascade compared to experimental oil flow visualization (*middle*). (Yp – loss coefficient).

value of $Yp = 0.097$. The simulation with the transition model gives a value of $Yp = 0.11$ in much closer agreement with the experiment. More turbomachinery-related test cases can be found in Langtry et al. [6], including an unsteady rotor-stator interaction simulation.

4.3. Wind turbine test case

The test case geometry is a 2D airfoil section, as typically used for GE wind-turbine blades. It operates in a low FSTI environment with a turbulence intensity of only around 0.1% at the leading edge. As a result, natural transition occurs on both the suction and pressure surfaces. The inlet value for the ω in this application was chosen to match the experimental transition location at 0° angle of attack. All other angles of attack have been computed with the identical settings. For a detailed discussion, see Langtry et al. [5].

The transition locations vs. angle of attack for the present transition model are shown in Figure 9 (left). Wind tunnel results and predictions XFOIL (v6.8) based on an e^n method are plotted for comparison. The experimental data were obtained using

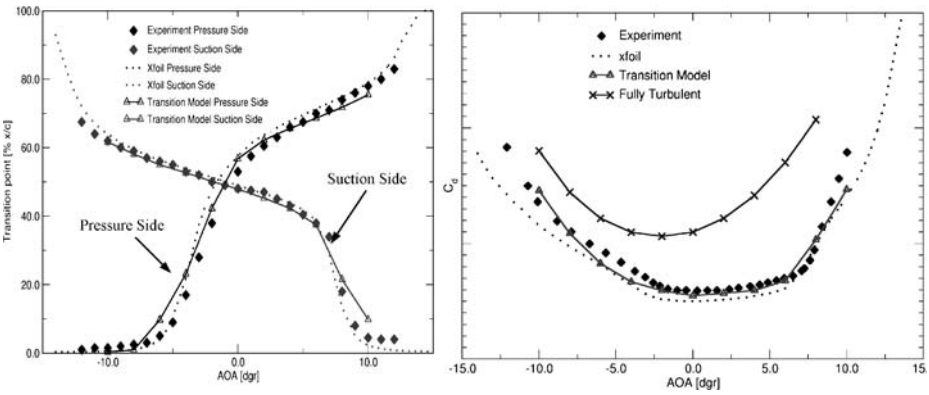

Figure 9 Predicted transition location (*left*) and drag coefficient (*right*) as a function of angle of attack for a wind turbine airfoil in comparison with experiments and the e^n-method used in XFOIL.

a stethoscope method. The current model captures the dependence of the transition location on the angle of attack in very good agreement with the data. The effect of the transition model is clearly visible also in the drag coefficient Figure 9 (right). Numbers could not be provided on the *y* axis, due to data confidentiality.

4.3.1. *3D NREL wind turbine simulation*

Simulations have been carried out for the NREL wind turbine [26]. This is a notoriously difficult test case to compute with CFD and a detailed comparison of CFD and experimental data is beyond the scope of this paper. However, in the simulation of this flow, it turned out that some interesting differences were observed between fully turbulent and transitional results at severe stall conditions.

The suction side intermittency predicted by the transitional CFD computations for wind speeds of 7, 10 and 20 m/s are shown in Figure 10. As the wind speed is increased the effective angle of attack of the wind turbine increases. For the 7 m/s wind speed the flow is largely attached on the suction side. In addition, a significant amount of laminar flow is predicted near the tip as well as in the hub region. In the tip region transition occurs at the 0.5 chord position whereas in the middle of the blade span transition occurs near the leading edge. This is most likely caused by the smaller radius resulting in an increased effective angle of attack. For the 10 m/s case, the inner hub region stalls while the tip region remains attached up until the 0.5 chord position. As well, due to the increased angle of attack the transition location near the tip moves to the leading edge. Finally, at 20 m/s the suction side of the blade is completely separated and the intermittency contours indicate that the flow is almost completely turbulent.

Figure 11 shows the shaft torque in comparison with experiments (left) and the flow topologies computed for fully turbulent and transitional settings. At a wind speed of 20 m/s, the flow topology computed with the fully turbulent and the transitional approaches are very different. This results in an 80% change in output torque. The lower output torque appears to be the result of a laminar separation in the leading edge region of the suction side of the blade. The transitional simulation is in much closer agreement with the experimental data.

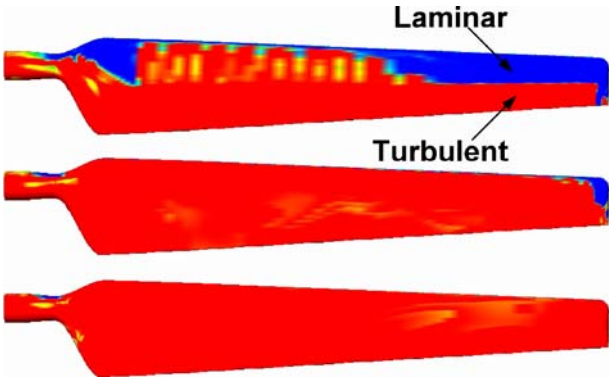

Figure 10 NREL wind turbine, suction surface intermittency computed by the transition model for wind speeds of 7 m/s (*top*), 10 m/s (*middle*) and 20 m/s (*bottom*).

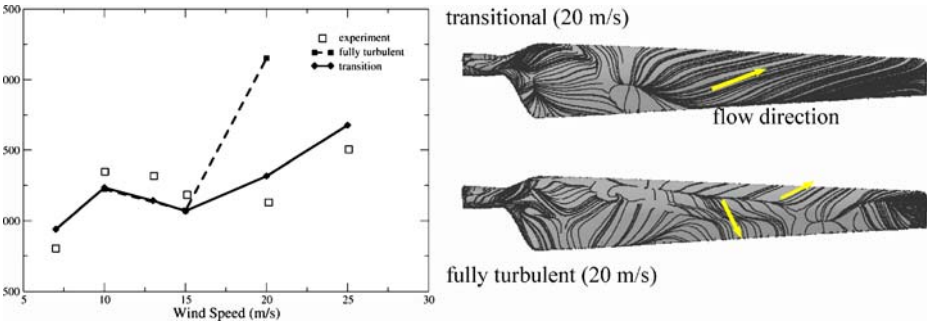

Figure 11 Shaft torque at different wind speeds (*left*). Flow topology on suction side for fully turbulent and transitional simulations (*right*).

4.3.2. *Aeronautical test cases*

Transition in aeronautical flows is typically a result of Tollmien–Schlichting waves or a crossflow instability. The current model does presently not include correlations for crossflow instabilities. It does however account for natural transition including pressure gradients. For more details on the test cases see Langtry and Menter [7].

4.3.3. *McDonald Douglas 30P–30N flap*

The McDonald Douglas 30P–30N flap configuration was originally a test case for the High-Lift Workshop/CFD Challenge that was held at the NASA Langley Research Center in 1993 [4]. It is a very complex test case for a transition model because of the large changes in pressure gradient and the varying local free-stream turbulence intensity around the different lifting surfaces.

The experiment was performed in the Langley Low Turbulence Pressure Tunnel and the transition locations were measured using hot films on the upper surface of the slat and flap and on both the upper and lower surfaces of the main element. The skin friction was also measured at various locations using a Preston tube [4]. For the present comparison the Reynolds number $Re = 9 \times 10^6$ and an angle of attack $\alpha = 8°$ was selected. The free-stream conditions for k and ω were selected to match the transition location at the suction side of the slat. The other transition locations are an outcome of the simulation.

A contour plot of the predicted turbulence intensity around the flap is shown in Figure 12. Also indicated are the various transition locations that were measured in the experiment (Exp.) as well as the locations predicted by the present transition model (CFD). In the computations, the onset of transition was judged as the location were the skin friction first started to increase due to the production of turbulent kinetic energy in the boundary layer. In general the agreement between the measured and predicted transition locations is very good. The largest error was observed on the lower surface of the main element where the predicted transition location was too far downstream by approximately 6% of the cruise-airfoil chord.

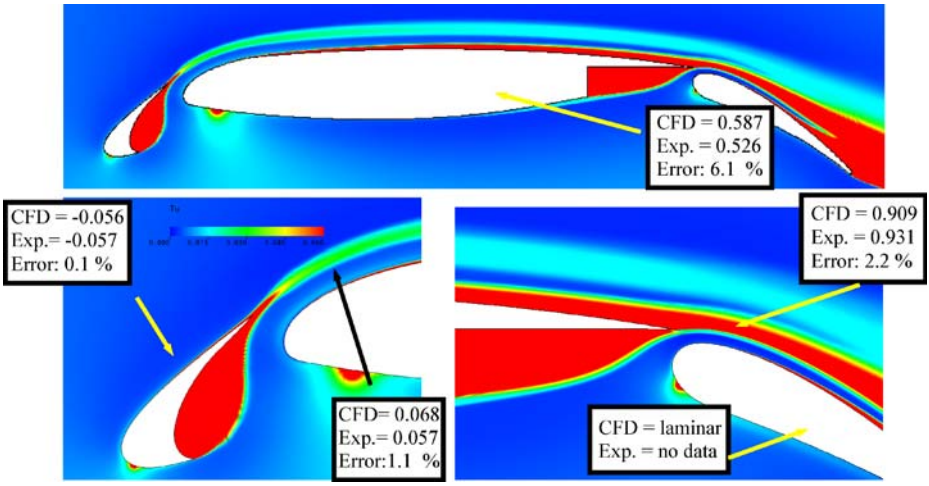

Figure 12 Contour of turbulence intensity (*Tu*) around the McDonald Douglas 30P-30N flap as well as the measured (*Exp.*) and predicted (*CFD*) transition locations (x/c) as a function of the cruise-airfoil chord ($c = 0.5588$ m). Also indicated is the relative error between the experiment and the predictions.

4.3.4. *DLR F-5 wing*

The DLR F-5 geometry is a 20° swept wing with a symmetrical airfoil section that is supercritical at a free-stream Mach number of 0.82. The experiment was performed at the DLR by Sobieczky [28] and consists of a wing mounted to the tunnel sidewall (which is assumed to have transitioned far upstream of the wing). At the root the wing was designed to blend smoothly into the wall thus eliminating the horseshoe vortex that usually develops there. The experimental measurements consist of wing mounted static taps at various span wise locations and flow visualization of the surface shear using a sublimation technique. The experimental flow visualization is shown in Figure 13 (right). Based on the flow visualization and the pressure measurements a diagram of the flow field around the wing was constructed and can be seen in Figure 13 (middle). From the measurements the boundary layer is laminar until about 60% chord where a shock causes the laminar boundary layer to separate and reattach as a turbulent boundary layer. The contours of skin friction and the surface streamlines predicted by the transition model are shown in Figure 13 (left). From the skin friction the laminar separation and turbulent reattachment can be clearly seen and both appear to be in good agreement with the experimental diagram from about 20% span out to the wing tip. Near the wing-body intersection, the experiments indicate earlier transition than the simulations. This might be due to the omission of the crossflow instability in the transition model.

4.3.5. *Eurocopter cabin*

The helicopter test case was investigated to demonstrate the model's ability of solving flows around complex geometries including multiple physical effects. There are no experimental data available in the public domain, which precludes the use of the

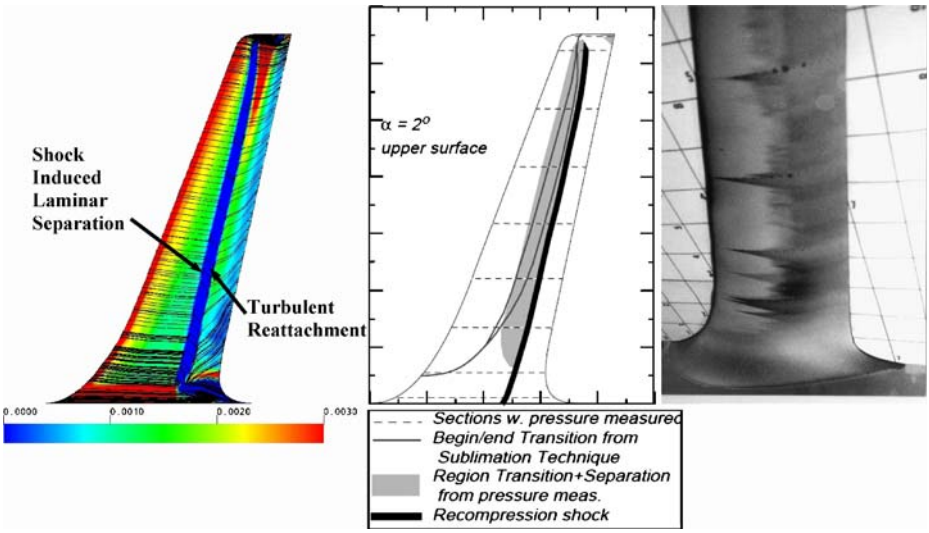

Figure 13 DLR-F5 wing with transition. Simulations (*left*); experiment (*middle* and *right*). Note: What is labeled a recompression shock in the experiment is most likely due to the strong pressure change associated with a reattaching boundary layer.

test case for model validation. Nevertheless, interesting transitional phenomena can be observed. In addition, the numerical performance of the transition model can be investigated.

The grid for this case consisted of about 6 million nodes and each solution was run overnight in parallel on a 16 CPU 1.5 Ghz Linux cluster. The convergence of lift and drag is shown in Figure 14 for the fully turbulent (top) and transitional (bottom) solutions. The transition model does not appear to have any adverse effects on the convergence and converges similar to the fully turbulent solution. This was

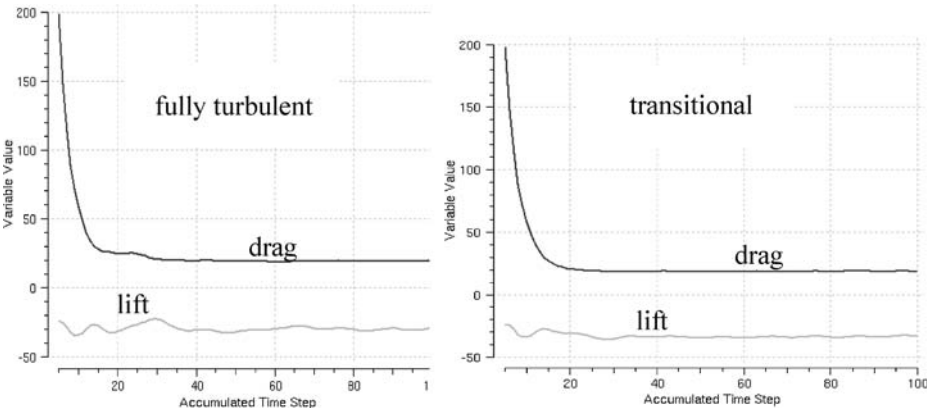

Figure 14 Convergence of lift and drag for the fully turbulent (*left*) and transitional (*right*) Eurocopter simulation.

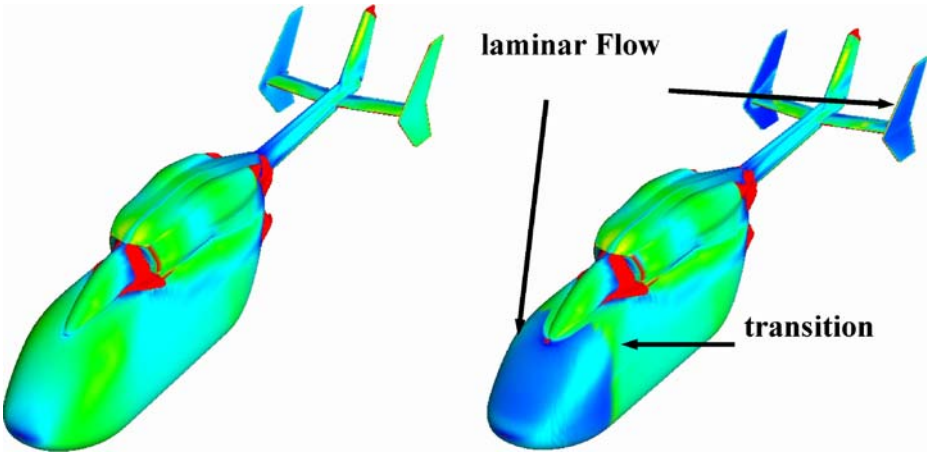

Figure 15 Contour plot of skin friction for a fully turbulent (*left*) and transitional (*right*) solution of the Eurocopter cabin. Isosurface indicates reverse flow.

also observed in most of the other cases. Typically the convergence is somewhat reduced in the transitional simulations, as the transition location has to settle down before convergence can be reached. The overall increase (additional equations and convergence) of the model is typically ∼20%. The transitional flow on the fuselage and tails resulted in a 5% drag reduction compared to the fully turbulent solution.

The predicted skin friction for a fully turbulent and transitional solution is shown in Figure 15. The main differences in the transitional solution are that the front part of the fuselage, the two outside vertical tail surfaces and the outer half of the horizontal tail surface are laminar. The fact that the transition model predicted turbulent flow on the middle vertical stabilizer and the inner part of the horizontal stabilizer was unexpected. Further investigation revealed that this was caused by the turbulent wake that was shed from the fuselage upstream of the tail. This is best illustrated in Figure 16. The left picture shows an iso-surface of the turbulent flow. The turbulent wake is clearly visible and can be seen passing over the middle vertical stabilizer and the inner part of the horizontal stabilizer. Consequently, the transition

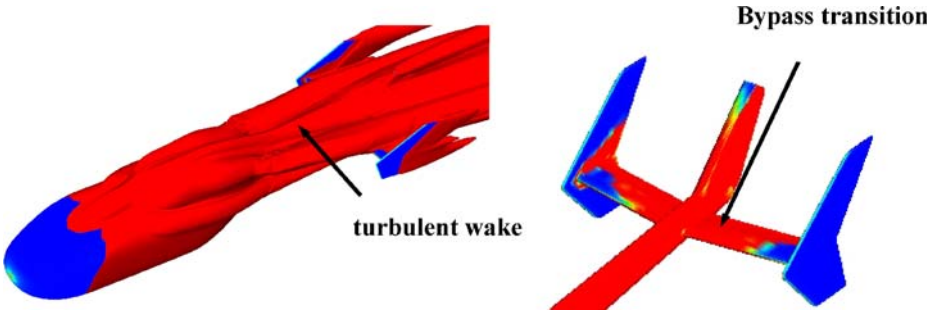

Figure 16 Iso-surface of turbulent flow (*left*) and surface value of intermittency (*right*) indicating the laminar (*blue*) and turbulent (*red*) regions on the Eurocopter airframe.

model predicts bypass transition on these surfaces due to the high local free-stream turbulence intensity from the wake.

The Eurocopter test case demonstrates the potential of the transition model for solving complex aerodynamic flow problems, with the inclusion of first order transitional effects. Further model refinements are required for calibration of the model for such flows, including a model extension for crossflow instability.

5. Conclusions

Methods for transition prediction in general purpose CFD codes have been discussed. The requirements, which a model has to satisfy to be suitable for implementation into such a code, have been listed. The main criterion is that nonlocal operations must be avoided. A new concept of transition modeling termed Local Correlation-based Transition Model (LCTM) was introduced. It combines the advantages of locally formulated transport equations with the physical information contained in empirical correlations. The γ-Re_θ transition model is a representative of that modeling concept. The model is based on two transport equations, one for intermittency and one for a transition onset criterion in terms of momentum thickness Reynolds number. The proposed transport equations do not attempt to model the physics of the transition process (unlike, e.g., turbulence models), but form a framework for the implementation of transition correlations into general-purpose CFD methods.

An overview of the γ-Re_θ model formulation has been given and numerous test cases have been computed successfully. The authors believe that the current model is a significant step forward in engineering transition modeling. Because it is based on transport equations, the model formulation therefore offers a flexible environment for engineering transition predictions that is fully compatible with the infrastructure of modern CFD methods. As a result, the model can be used in any general purpose CFD method without special provisions for geometry and grid topology.

The present transition model accounts for transition due to free-stream turbulence intensity, pressure gradients and separation. It is fully CFD-compatible and does not negatively affect the convergence of the solver. Current limitations of the model are that crossflow instability is not included in the correlations and that the transition correlations are formulated non-Galilean invariant. Both limitations are currently being investigated and can be removed in principle. Another area for future investigations is the important effect of wake induced transition, as it occurs on blades of axial turbines/compressors affected by the wake of upstream blade rows. The helicopter test case shows that wake-induced transition can be handled by the model. The increased FSTI caused by the wake, affects the transition onset correlation, leading to earlier transition. Tests for unsteady turbomachinery cases are required for further validation of this functionality.

An overview of the test cases computed with the new model has been given. Due to the nature of the paper, the presentation of each individual test case had to be brief. More details on the test case set-up, boundary conditions grid resolutions etc. can be found in the cited papers. The purpose of the overview was to show that the model can handle a wide variety of geometries and physically diverse problems. The authors believe that the LCTM concept of combining transition correlations with locally formulated transport equations has a strong potential for allowing the 1st order effects of transition to be included into today's industrial CFD simulations.

Acknowledgement The model development and validation at ANSYS CFX was funded by GE Aircraft Engines and GE Global Research. Prof. G. Huang and Dr B. Suzen from the University of Kentucky have supported the original model development with their extensive know-how and their in-house codes.

References

1. Abu-Ghannam, B.J., Shaw, R.: Natural transition of boundary layers – the effects of turbulence, pressure gradient and flow history. J. Mech. Eng. Sci. **22**, 213–228 (1980)
2. Arts, T., Lambert de Rouvroit, M., Rutherford, A.W.: Aero-thermal Investigation of a Highly Loaded Transonic Linear Turbine Guide Vane Cascade. von Karman Institute for Fluid Dynamics, Technical Note 174 (1990)
3. Jones, W.P., Launder, B.E.: The calculation of low Reynolds number phenomena with a two-equation model of turbulence. Int. J. Heat Mass Transfer **15**, 301–314 (1973)
4. Klausmeyer, S.M., Lin, J.C.: Comparative Results From a CFD Challenge Over a 2D Three-element High-Lift Airfoil. NASA Technical Memorandum 112858 (1997)
5. Langtry, R.B., Gola, J., Menter, F.R.: Predicting 2D Airfoil and 3D Wind Turbine Rotor Performance using a Transition Model for General CFD Codes, AIAA Paper 2006-0395, 44th AIAA Aerospace Sciences Meeting and Exhibit, Reno NV (2006)
6. Langtry, R.B., Menter, F.R., Likki, S.R., Suzen, Y.B., Huang, P.G., Völker, S.: A Correlation based Transition Model using Local Variables Part 2 – Test Cases and Industrial Applications. ASME-GT2004-53454, ASME TURBO EXPO 2004, Vienna, Austria (2004)
7. Langtry, R.B., Menter, F.R.: Transition Modeling for General CFD Applications in Aeronautics, AIAA Paper 2005-522, Reno, Nevada (2005)
8. Langtry, R.B., Sjolander, S.A.: Prediction of Transition for Attached and Separated Shear Layers in Turbomachinery. In: AIAA-2002-3643, 38th AIAA/ASME/SAE/ASEE Joint Propulsion Conference and Exhibit (2002)
9. Lardeau, S., Leschziner, M.A., Li, N.: Modelling bypass transition with low-Reynolds-number nonlinear Eddy-viscosity closure. Flow Turbul. Combust. **73**, 49–76 (2004)
10. Mayle, R.E.: The role of laminar-turbulent transition in gas turbine engines. J. Turbomach. **113**, 509–537 (1991)
11. Mayle, R.E., Schulz, A.: The path to predicting bypass transition. ASME J. Turbomach. **119**, 405–411 (1997)
12. Mayle, R.E.: Transition in a separation bubble. J. Turbomach. **118**, 752–759 (1996)
13. McIlroy, H.M., Budwig, R.S.: The boundary layer over turbine blade models with realistic rough surfaces. ASME-GT2005-68342, ASME TURBO EXPO 2005, Reno-Tahoe, Nevada, USA (2005)
14. Menter, F.R.: Two-equation Eddy-viscosity turbulence models for engineering applications. AIAA J. **32**(8), 1598–1605 (1994)
15. Menter, F.R., Esch, T., Kubacki, S.: Transition modelling based on local variables. In: 5th International Symposium on Turbulence Modeling and Measurements, Mallorca, Spain (2002)
16. Menter, F.R., Langtry, R.B., Likki, S.R., Suzen, Y.B., Huang, P.G., Völker, S.: A correlation based transition model using local variables part 1 – model formulation. In: ASME-GT2004-53452, ASME TURBO EXPO 2004, Vienna, Austria (2004)
17. Michelassi, V., Wissink, J.G., Rodi, W.: Analysis of DNS and LES of flow in a low pressure turbine cascade with incoming wakes and comparison with experiments. Flow Turbul. Combust. **69**, 295–330 (2002)
18. Morkovin, M.V.: On the many faces of transition. In: Wells, C.S. (ed.) Viscous Drag Reduction, pp 1–31. Plenum, New York (1969)
19. Rodi, W., Scheuerer, G.: Calculation of laminar-turbulent boundary layer transition on turbine blades. In: AGARD CP 390 on Heat transfer and Cooling in Gas Turbines, 18-1 (1984)
20. Savill, A.M.: Some recent progress in the turbulence modelling of by-pass transition. In: So, R.M.C., Speziale, C.G., Launder, B.E. (eds.) Near-Wall Turbulent Flows. Elsevier, The Netherlands, p. 829 (1993)
21. Savill, A.M.: One-point closures applied to transition. In: Hallbäck, M., et al. (eds.) Turbulence and Transition Modelling, pp. 233–268. Kluwer, Dordrecht (1996)

22. Savill, A.M.: By-Pass Transition using Conventional Closures. In: Launder, B.E., Sandham, N.D. (eds.) Closure Strategies for Turbulent and Transitional Flows, Ch. 17, pp. 464–492. Cambridge University Press, Cambridge (2002)
23. Savill, A.M.: New strategies in modelling by-pass transition. In: Launder, B.E., Sandham, N.D. (eds.) Closure Strategies for Turbulent and Transitional Flows, Ch. 18, pp. 492–521. Cambridge University Press, Cambridge (2002)
24. Schubauer, G.B., Klebanoff, P.S.: Contribution on the Mechanics of Boundary Layer Transition. NACA TN 3489 (1955)
25. Schulz, H.D., Gallus, H.D.: Experimental investigation of the three-dimensional flow in an annular compressor cascade. ASME J. Turbomach. **110**, (October 1988)
26. Simms, D., Schreck, S., Hand, M, Fingersh, L.J.: NREL Unsteady Aerodynamics Experiment in the NASA-Ames Wind Tunnel: A Comparison of Predictions to Measurements. NREL Technical report, NREL/TP-500-29494 (2001)
27. Smith, A.M.O., Gamberoni, N.: Transition, Pressure Gradient and Stability Theory. Douglas Aircraft Company, Long Beach, California Rep. ES 26388 (1956)
28. Sobieczky, H.: DLR – F5: Test Wing for CFD and Applied Aerodynamics, Test Case B-5 in AGARD FDP Advisory Report AR 303: Test Cases for CFD Validation (1994)
29. Steelant, J., Dick, E.: Modeling of bypass transition with conditioned Navier-Stokes equations coupled to an intermittency transport equation. Int. J. Num. Methods Fluids **23**, 193–220 (1996)
30. Steelant, J., Dick, E.: Modeling of laminar-turbulent transition for high freestream turbulence. J. Fluids Eng. **123**, 22–30 (2001)
31. Stock, H.W., Haase, W.: Navier–Stokes airfoil computations with e^N transition prediction including transitional flow regions. AIAA J. **38**(11), 2059–2066 (2000)
32. Suzen, Y.B., Huang, P.G.: Modeling of flow transition using an intermittency transport equation. J. Fluids Eng. **122**, 273–284 (2000)
33. Suzen, Y.B., Xiong, G., Huang, P.G.: Predictions of transitional flows in low-pressure turbines using an intermittency transport equation. AIAA J. **40**, 254–266 (2002)
34. Suzen, Y.B., Huang, P.G., Hultgren, L.S., Ashpis, D.E.: Predictions of separated and transitional boundary layers under low-pressure turbine airfoil conditions using an intermittency transport equation. J. Turbomach. **125**(3), 455–464 (July 2003)
35. Van Driest, E.R., Blumer, C.B.: Boundary layer transition: Freestream turbulence and pressure gradient effects. AIAA J. **1**(6), 1303–1306 (1963)
36. Van Ingen, J.L.: A suggested semi-empirical method for the calculation of the boundary layer transition region. Univ. of Delft, Dept. Aerospace Engineering, Delft, The Netherlands, Rep. VTH-74 (1956)
37. Walters, D.K, Leylek, J.H.: A new model for boundary-layer transition using a single-point Rans approach. J. Turbomach. **126**, 193–202 (2004)
38. Wilcox, D.C.W.: Simulation of transition with a two-equation turbulence model. AIAA J. **32**(2) (1994)
39. Wu, X., Jacobs, R., Hunt, J., Durbin, P.: Simulation of boundary layer transition induced by periodically passing wakes. J. Fluid Mech. **398**, 109–153 (1999)
40. Zierke, W.C., Deutsch, S.: The Measurement of Boundary Layers on a Compressor Blade in Cascade – Vols. 1 and 2. *NASA CR 185118* (1989)